Quantum-kinetic theory of steady-state photocurrent generation in thin films: Coherent versus incoherent coupling

U. Aeberhard*
IEK-5: Photovoltaik, Forschungszentrum Jülich, D-52425 Jülich, Germany
(Dated: February 26, 2014)

The generation of photocurrents due to coupling of electrons to both classical and quantized electromagnetic fields in thin semiconductor films is described within the framework of the nonequilibrium Green's function formalism. For the coherent coupling to classical fields corresponding to single field operator averages, an effective two-time intraband self-energy is derived from a band decoupling procedure. The evaluation of coherent photogeneration is performed self-consistently with the propagation of the fields by using for the latter a transfer matrix formalism with an extinction coefficient derived from the electronic Green's functions. For the "incoherent" coupling to fluctuations of the quantized fields, which need to be considered for the inclusion of spontaneous emission, the first self-consistent Born self-energy is used, with full spatial resolution in the photon Green's functions. These are obtained from the numerical solution of Dyson and Keldysh equations including a nonlocal photon self-energy based on the same interband polarization function as used for the coherent case. A comparison of the spectral and integral photocurrent generation pattern reveals a close agreement between coherent and incoherent coupling for the case of an ultra-thin, selectively contacted absorber layer at short circuit conditions.

PACS numbers: 72.20.Jv, 72.40.+w, 78.20.-e, 78.20.Bh, 78.56.-a

I. INTRODUCTION

Among the state-of-the-art theories used to describe the operation of complex nanostructure-based optoelectronic devices, e.g., quantum well and quantum dot lasers and light-emitting diodes, quantum-kinetic formalisms are most powerful in terms of both physical insight and predictive power provided[1]. However, the simulation of devices such as nanostructure-based solar cells requires the development of a unified picture of quantum optics and quantum transport[2], since an accurate description of both optics and charge transport is crucial to capture the impact of complex dielectric and electronic nanostructure potentials on the device performance[3]. There, one is faced with the problem of different representations of the quantum-kinetic theory conventionally used. In quantum optics, the focus is on transient or ultrafast phenomena, with standard descriptions based on density matrix theory corresponding to the equal time Green's function formalism[4,5]. In quantum transport, the operating regime of interest is the steady state, which on the quantum-kinetic level is described by using the Fourier transform to the energy domain of the relative time in the two-time Green's function[6,7].

In this paper, two different approaches to the solution of the problem are presented. Both are concerned with the formulation of an electron-photon self-energy compatible with the steady-state non-equilibrium Green's function (NEGF) formalism of quantum transport. In the first case, the self-energy describes the coupling of the electronic system to coherent fields as obtained from classical solutions of Maxwell's equations. It establishes the connection to conventional description of light attenuation in solar cells and provides a computationally efficient treatment of stimulated electron-photon processes within the NEGF formalism. The second type of electron-photon self-energy relates to the non-local photon Green's function (GF) on the level of quantum statistical mechanics and includes the coupling to incoherent field fluctuations. It enables a consistent description of optical generation and radiative recombination by including the coupling to any available photon modes of the device, from the leaky modes occupied by incident solar photons to the guided modes populated by spontaneous emission. This is an essential prerequisite for the assessment of the radiative efficiency limit in novel nanostructure-based solar cell devices.

The paper is organized as follows. After the formulation of the general NEGF theory of optoelectronic processes for a two-band semiconductor model in Sec. II, the effective self-energy for coherent coupling is derived in Sec. III. The main body of the paper is formed by Sec. IV on the application of the NEGF theory to the simulation of charge carrier photogeneration in thin semiconductor films for coupling to classical, average fields and to the non-equilibrium statistical ensemble average of field operator pairs. For both classical and quantized fields, expressions for the local photogeneration rate, the local absorption coefficient and the absorptance, as well as the resulting photocurrent, are formulated in the microscopic NEGF picture and evaluated via numerical simulation for a prototypical thin-film solar cell architecture.

II. QUANTUM-KINETIC THEORY OF ELECTRON-PHOTON INTERACTION IN A TWO BAND MODEL

The electronic model system under investigation is a simple two band model of a direct gap semiconductor

film furnished with ohmic contacts and coupled to an external photon field[8], which is treated either classically or quantum mechanically. The Hamiltonian of the electronic system thus reads

$$\hat{H} = \hat{H}_0 + \hat{H}_{e\gamma} + \hat{H}_C + \hat{H}_{diss}. \tag{1}$$

$\hat{H}_0$ is the Hamiltonian of the noninteracting isolated mesoscopic absorber plus the Hartree term $U(\mathbf{r})$ from the solution of the macroscopic Poisson equation, corresponding to a mean-field treatment of carrier-carrier interaction. $\hat{H}_{e\gamma}$ describes the light-matter interaction and $\hat{H}_C$ the (selective) coupling to contacts. At this level, the theory is able to cover the operation of an ideal solar cell. The generic term $\hat{H}_{diss}$ encodes dissipative processes such as electron-phonon interaction as well as non-radiative recombination processes and is not considered here. The carriers in conduction (c) and valence (v) bands are described by field operators $\hat{\Psi}_b(\mathbf{r}, t)$, $b = c, v$, defining the charge carrier Green's functions via

$$G_{ab}(\underline{1}, \underline{1}') \equiv -\frac{i}{\hbar}\langle \hat{\Psi}_a(\underline{1})\hat{\Psi}_b^\dagger(\underline{1}')\rangle_{\mathcal{C}} \tag{2}$$

for band indices $\{a, b\} \in \{c, v\}$ and $\underline{1} \equiv (\mathbf{r}_1, \underline{t}_1 \in \mathcal{C})$, where $\mathcal{C}$ denotes the Keldysh contour[9]. The electromagnetic field is described in terms of the vector potential operator, $\hat{\mathbf{A}} = \hat{\mathbf{A}}_{coh} + \hat{\mathbf{A}}_{inc}$ which is decomposed into a coherent contribution $\hat{\mathbf{A}}_{coh}$ corresponding to coherent light sources and a contribution $\hat{\mathbf{A}}_{inc}$ from incoherent light sources and from spontaneous emission. The coherent vector potential is related to the time-dependent part of the classical electric field $\boldsymbol{\mathcal{E}}$ via the standard relation

$$-\frac{\partial}{\partial t}\langle \hat{\mathbf{A}}_{coh}(\mathbf{r}, \underline{t})\rangle_{\mathcal{C}} = \boldsymbol{\mathcal{E}}(\mathbf{r}, t). \tag{3}$$

The photon Green's function $\mathcal{D}$, on the other hand, includes the incoherent field fluctuations[10],

$$\mathcal{D}_{\mu\nu}(\underline{1}, \underline{2}) = -\frac{i}{\mu_0\hbar}\left[\langle \hat{A}_\mu(\underline{1})\hat{A}_\nu(\underline{2})\rangle_{\mathcal{C}} - \langle \hat{A}_\mu(\underline{1})\rangle_{\mathcal{C}}\langle \hat{A}_\nu(\underline{2})\rangle_{\mathcal{C}}\right], \tag{4}$$

where μ_0 is the magnetic vacuum permeability.

In terms of the above field operators, the electron-photon coupling component in the Hamiltonian for the electronic system is expressed as follows:

$$[\mathcal{H}_{e\gamma}]_{ab}(t) = \int d^3r \hat{\Psi}_a^\dagger(\mathbf{r}, t)\hat{H}_{e\gamma}(\mathbf{r}, t)\hat{\Psi}_b(\mathbf{r}, t), \tag{5}$$

$$\hat{H}_{e\gamma}(\mathbf{r}, t) = -\frac{e}{m_0}\hat{\mathbf{A}}(\mathbf{r}, t)\cdot\hat{\mathbf{p}}. \tag{6}$$

In the NEGF picture of photogeneration, the effect of irradiation on the electronic system is considered in the form of a self-energy that renormalizes the carrier Green's function in the solution of the Dyson equations. For weak coupling, the self-energy can be derived within many-body perturbation theory using the Hamiltonian (5), from the expansion of the perturbed (photon assisted) carrier Green's function

$$G(\mathbf{r}, t; \mathbf{r}', t') = -\frac{i}{\hbar}\left\langle e^{-\frac{i}{\hbar}\int_{\mathcal{C}} ds \hat{\mathcal{H}}_{e\gamma}(s)}\hat{\Psi}(\mathbf{r}, \underline{t})\hat{\Psi}^\dagger(\mathbf{r}', \underline{t}')\right\rangle_{\mathcal{C}}. \tag{7}$$

To first order in the vector potential, perturbation theory results in the singular self-energy term

$$\Sigma^{\delta}_{e\gamma}(\underline{1}) = -\frac{e}{m_0}\langle \hat{\mathbf{A}}(\underline{1})\rangle_{\mathcal{C}}\cdot\hat{\mathbf{p}}(1) \equiv -\frac{e}{m_0}\hat{\mathbf{A}}_{coh}(\underline{1})\cdot\hat{\mathbf{p}}(1), \tag{8}$$

which corresponds to the interband term in the effective Hamiltonian originating in the coupling to transverse photons. To second order in the vector potential, the self-energy corresponds to the random phase approximation (RPA) expression[11,12]

$$\Sigma^{RPA}(\underline{1}, \underline{2}) = i\hbar\mu_0\Big(\frac{e}{m_0}\Big)^2 \sum_{\mu\nu}\hat{p}^\mu(1, 1')G(\underline{1}, \underline{2}) \times \hat{p}^\nu(2)\mathcal{D}_{\mu\nu}(\underline{2}, \underline{1}')|_{1'=1}, \tag{9}$$

where $\hat{p}$ is the momentum operator and $\hat{p}^\mu(1, 1') \equiv [\hat{p}^\mu(1) - \hat{p}^\mu(1')]/2$. This self-energy can also be derived via functional derivative techniques[13–15]. The photon Green's functions in (9) are obtained from the corresponding Dyson equations[15,16]:

$$\int_{\mathcal{C}} d3\left[\mathcal{D}^{-1}_{0,\mu\nu}(\underline{1}, \underline{3}) - \Pi_{\mu\beta}(\underline{1}, \underline{3})\right]\mathcal{D}_{\beta\nu}(\underline{3}, \underline{2}) = \delta_{\parallel,\mu\nu}(\underline{1}, \underline{2}), \tag{10}$$

where $\mathcal{D}_{0,\mu\nu}$ is the free propagator defined by

$$\mathcal{D}^{-1}_{0,\mu\nu}(\underline{1}, \underline{2}) = \left[\Delta_1 - \frac{1}{c^2}\frac{\partial^2}{\partial t_1^2}\right]\delta_{\mu\nu}\delta(\underline{1}, \underline{2}), \tag{11}$$

and $\delta_{\parallel,\mu\nu}(\underline{1}, \underline{2}) = \delta(\underline{t}_1 - \underline{t}_2)\delta_{\parallel,\mu\nu}(\mathbf{r}_1 - \mathbf{r}_2)$ is the transverse δ function. In Eq. (10), $\mathbf{\Pi}$ is the photon self-energy describing the renormalization of the photon Green's function due to interaction with the electronic system. The RPA photon self energy due to interband transitions[17] is given in terms of electronic Green's functions and momentum operator elements as follows[11,12]:

$$\Pi^{RPA}_{\mu\nu}(\underline{1}, \underline{2}) = -i\hbar\mu_0\Big(\frac{e}{m_0}\Big)^2\hat{p}^\mu(1, 1')G(\underline{1}, \underline{2}) \times \hat{p}^\nu(2)G(\underline{2}, \underline{1}')|_{1'=1}. \tag{12}$$

For the comparison of the two types of electron-photon self-energies, the effects of the singular interband term needs to be transferred to an effective two-time intraband self-energy, which can be achieved via a band decoupling procedure, as shown below.

III. EFFECTIVE INTERBAND SELF-ENERGY FOR COHERENT COUPLING

In the following, a band decoupling scheme similar to that introduced in Ref. 18 will be applied to the two

band model. The procedure was given in the appendix of Ref. 19 for a general singular self-energy term, but for the sake of clarity and completeness will be repeated here for the specific case of the electron-photon interaction.[20] Starting point are the Kadanoff-Baym equations for contour-ordered non-equilibrium Green's functions[21],

$$\mathbf{G}_0^{-1}(\underline{1},\underline{1})\mathbf{G}(\underline{1},\underline{1}') = \boldsymbol{\delta}(\underline{1},\underline{1}') + \int_{\mathcal{C}} \mathrm{d}2\, \mathbf{\Sigma}(\underline{1},\underline{2})\mathbf{G}(\underline{2},\underline{1}'), \tag{13}$$

$$[\mathbf{G}_0^{\dagger}]^{-1}(\underline{1}',\underline{1}')\mathbf{G}(\underline{1},\underline{1}') = \boldsymbol{\delta}(\underline{1},\underline{1}') + \int_{\mathcal{C}} \mathrm{d}2\, \mathbf{G}(\underline{1},\underline{2})\mathbf{\Sigma}(\underline{2},\underline{1}'), \tag{14}$$

where

$$[G_0^{-1}(\underline{1},\underline{1}')]_{ab} = \left(i\hbar\frac{\partial}{\partial t_1} - [H_0(\mathbf{r}_1)]_a\right)\delta(\underline{1},\underline{1}')\delta_{ab}, \tag{15}$$

and G_{ab} is defined in (2). Real-time decomposition rules[22] applied to (13) provide the coupled equations for the retarded components of the intra- and interband Green's functions,

$$G_{0,cc}^{-1}(1,1)G_{cc}^R(1,1') = \delta(1,1') + \Sigma_{cv}^{\delta}(1)G_{vc}^R(1,1') + \int \mathrm{d}2\, \Sigma_{cc}^R(1,2)G_{cc}^R(2,1'), \tag{16}$$

$$G_{0,vv}^{-1}(1,1)G_{vc}^R(1,1') = \Sigma_{vc}^{\delta}(1)G_{cc}^R(1,1') + \int \mathrm{d}2\, \Sigma_{vv}^R(1,2)G_{vc}^R(2,1'). \tag{17}$$

Introducing the new quantity

$$\tilde{G}_{vv}^R \equiv \left[G_{0,vv}^{-1} - \Sigma_{vv}^R\right]^{-1} \tag{18}$$

in (17), the retarded interband GF can be written as

$$G_{vc}^R(1,1') = \int \mathrm{d}2\, \tilde{G}_{vv}^R(1,2)\Sigma_{vc}^{\delta}(2)G_{cc}^R(2,1'). \tag{19}$$

Inserting the above expression in (16) yields a closed equation for the intraband GF,

$$G_{cc}^R(1,1') = \Big[G_{0,cc}^{-1}(1,1') - \Sigma_{cc}^R(1,1') - \Sigma_{cv}^{\delta}(1)\tilde{G}_{vv}^R(1,1')\Sigma_{vc}^{\delta}(1')\Big]^{-1} \tag{20}$$

$$\equiv \left[\tilde{G}_{cc}^{-1}(1,1') - \tilde{\Sigma}_{cc}^R(1,1')\right]^{-1}, \tag{21}$$

where the effective band-coupling self-energy $\tilde{\Sigma}$ was defined,

$$\tilde{\Sigma}_{cc}^R(1,1') \equiv \Sigma_{cv}^{\delta}(1)\tilde{G}_{vv}^R(1,1')\Sigma_{vc}^{\delta}(1'). \tag{22}$$

Similarly, the lesser and greater components of the Green's functions can be decoupled: starting from

$$G_{0,cc}^{-1}(1,1)G_{cc}^<(1,1') = \Sigma_{cv}^{\delta}(1)G_{vc}^<(1,1') + \int \mathrm{d}2\, \Sigma_{cc}^R(1,2)G_{cc}^<(2,1') + \int \mathrm{d}2\, \Sigma_{cc}^<(1,2)G_{cc}^A(2,1'), \tag{23}$$

$$G_{0,vv}^{-1}(1,1)G_{vc}^<(1,1') = \Sigma_{vc}^{\delta}(1)G_{cc}^<(1,1') + \int \mathrm{d}2\, \Sigma_{vv}^R(1,2)G_{vc}^<(2,1') + \int \mathrm{d}2\, \Sigma_{vv}^<(1,2)G_{vc}^A(2,1'), \tag{24}$$

the interband correlation or coherent polarization function is written as

$$G_{vc}^<(1,1') = \int \mathrm{d}2\, \Big[\tilde{G}_{vv}^R(1,2)\Sigma_{vc}^{\delta}(2)G_{cc}^<(2,1') + \tilde{G}_{vv}^<(1,2)\Sigma_{vc}^{\delta}(2)G_{cc}^A(2,1')\Big], \tag{25}$$

where

$$\tilde{G}_{vv}^<(1,1') \equiv \int \mathrm{d}2 \int \mathrm{d}3\, \tilde{G}_{vv}^R(1,2)\Sigma_{vv}^<(2,3)\tilde{G}_{vv}^A(3,1') \tag{26}$$

was introduced. Replacing the interband term in (23) then yields the intraband correlation function

$$G_{cc}^<(1,1') = \int \mathrm{d}2 \int \mathrm{d}3\, G_{cc}^R(1,2)\Big[\Sigma_{cc}^<(2,3) + \tilde{\Sigma}_{cc}^<(2,3)\Big]G_{cc}^A(3,1') \tag{27}$$

with

$$\tilde{\Sigma}_{cc}^<(1,1') \equiv \Sigma_{cv}^{\delta}(1)\tilde{G}_{vv}^<(1,1')\Sigma_{vc}^{\delta}(1'). \tag{28}$$

The expressions for the valence band self-energy corrections are obtained from analogous derivations as

$$\tilde{\Sigma}_{vv}^{\alpha}(1,1') = \Sigma_{cv}^{\delta}(1)\tilde{G}_{cc}^{\alpha}(1,1')\Sigma_{cv}^{\delta}(1'), \quad \alpha = R, A, \lessgtr. \tag{29}$$

We can now evaluate the effective band-coupling self-energy expression using the singular interband self-energies due to the coupling to coherent radiation or classical fields given in the previous section [Eq. (8)] and compare it to the self-energy for the coupling to incoherent radiation [Eq.(9)]. In steady-state conditions, the dependence on microscopic time vanishes and the relative time dependence is Fourier transformed to the energy domain. As shown in Ref. 14, using the rotating wave approximation, the coherently driven interband self-energies have a combined time-dependence $\propto e^{\pm i\omega\tau}$, where the sign depends on the band index and $\tau = t_1 - t_2$

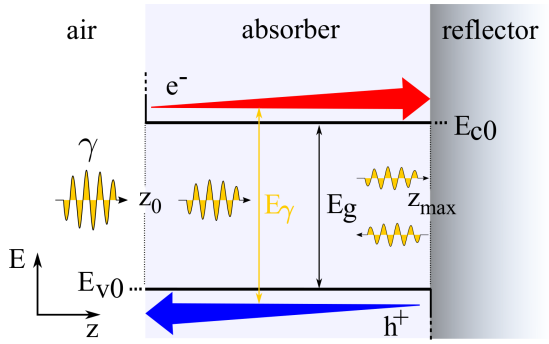

FIG. 1. (color online) Schematic band diagram representation of a flat band solar cell architecture with finite photocurrent flow enabled by carrier selective contacts: electrons (e^-) are blocked in the conduction band at $z = z_0$ via an infinite barrier potential in the conduction band energy E_C, while holes (h^+) are reflected at $z = z_{max}$ due to a similar barrier potential in E_V. For closer resemblance to actual thin-film solar cell configurations, an additional back reflector layer is considered in the optical simulations.

is the relative time, which provides the Fourier transform

$$\tilde{\Sigma}^{\lessgtr}_{cc}(\mathbf{r}_1,\mathbf{r}_2,E) = \int d\hbar\omega \Big[\Sigma^{\delta}_{cv}(\mathbf{r}_1,\hbar\omega) \times \int d\tau \tilde{G}^{\lessgtr}_{vv}(\mathbf{r}_1,\mathbf{r}_2,\tau) e^{\frac{i}{\hbar}(E-\hbar\omega)\tau}\Sigma^{\delta}_{vc}(\mathbf{r}_2,\hbar\omega)\Big] \tag{30}$$

$$= \int d\hbar\omega \Sigma^{\delta}_{cv}(\mathbf{r}_1,\hbar\omega)\tilde{G}^{\lessgtr}_{vv}(\mathbf{r}_1,\mathbf{r}_2,E-\hbar\omega)\Sigma^{\delta}_{vc}(\mathbf{r}_2,\hbar\omega), \tag{31}$$

and

$$\tilde{\Sigma}^{\lessgtr}_{vv}(\mathbf{r}_1,\mathbf{r}_2,E) = \int d\hbar\omega \Sigma^{\delta}_{vc}(\mathbf{r}_1,\hbar\omega) \times \tilde{G}^{\lessgtr}_{cc}(\mathbf{r}_1,\mathbf{r}_2,E+\hbar\omega)\Sigma^{\delta}_{cv}(\mathbf{r}_2,\hbar\omega). \tag{32}$$

Inserting the explicit form of the coherent singular self-energies (8) and integrating over photon energies $E_\gamma = \hbar\omega$ yields the general polychromatic expression

$$\tilde{\Sigma}^{\lessgtr}_{aa}(\mathbf{r}_1,\mathbf{r}_2,E) = \Big(\frac{e}{m_0}\Big)^2 \sum_{\mu\nu}\int dE_\gamma A_\mu(\mathbf{r}_1,E_\gamma)p^{\mu}_{ab}(\mathbf{r}_1) \times \tilde{G}^{\alpha}_{bb}(\mathbf{r}_1,\mathbf{r}_2,E\mp E_\gamma)A^*_\nu(\mathbf{r}_2,E_\gamma)p^{\nu *}_{ab}(\mathbf{r}_2), \tag{33}$$

where the negative sign is for $a = c$ and the electromagnetic vector potential is normalized to the total intensity, i.e., it has units $(\mathrm{eV})^{\frac{1}{2}}/(\mathrm{Am})$.

IV. PHOTOGENERATION IN THIN FILMS

A large variety of advanced optoelectronic devices with nanoscale active region are based on ultra-thin semiconductor films. Here, as a simple model system for the evaluation of electron-photon coupling, an intrinsic GaAs slab at short circuit conditions is used. Photocurrent rectification is achieved via the imposition of carrier selective contacts, which is sufficient for photovoltaic operation[23], and has already been applied in the NEGF simulation of nanostructured solar cells[24]. The architecture shown in Fig. 1 deviates minimally from the standard flat band bulk situation in terms of electronic structure, but provides at the same time complete charge separation. For the system to show more resemblance to the situation encountered in actual thin-film solar cell devices, a silver back reflector contact layer is added to the right of the slab for the optical simulation.

Before comparing the optoelectronic response of a given structure to classical and quantized fields, the representation of the NEGF formalism is adjusted to the slab system at hand.

A. Electronic and optical states in thin semiconductor films

In the layer structure with homogeneous transverse dimensions, the description of the optoelectronic properties can be simplified by using a plane wave expansion of the field operators for electrons and photons with respect to transverse coordinates, i.e.,

$$\hat{\Psi}(\mathbf{r},t) = \mathcal{A}^{-\frac{1}{2}}\sum_{\mathbf{k}_\parallel}\hat{\Psi}(\mathbf{k}_\parallel,z,t)e^{i\mathbf{k}_\parallel\cdot\mathbf{r}_\parallel}, \tag{34}$$

$$\hat{\mathbf{A}}(\mathbf{r},t) = \mathcal{A}^{-\frac{1}{2}}\sum_{\mathbf{q}_\parallel}\hat{\mathbf{A}}(\mathbf{q}_\parallel,z,t)e^{i\mathbf{q}_\parallel\cdot\mathbf{r}_\parallel}, \tag{35}$$

where $\mathcal{A}$ denotes the cross section area of the film. The corresponding slab representation for the steady-state Green's functions is obtained from

$$G(\mathbf{r},\mathbf{r}',E) = \mathcal{A}^{-1}\sum_{\mathbf{k}_\parallel}G(\mathbf{k}_\parallel,z,z',E)e^{i\mathbf{k}_\parallel\cdot(\mathbf{r}_\parallel-\mathbf{r}'_\parallel)}, \tag{36}$$

$$\mathcal{D}_{\mu\nu}(\mathbf{r},\mathbf{r}',E) = \mathcal{A}^{-1}\sum_{\mathbf{q}_\parallel}\mathcal{D}_{\mu\nu}(\mathbf{q}_\parallel,z,z',E)e^{i\mathbf{q}_\parallel\cdot(\mathbf{r}_\parallel-\mathbf{r}'_\parallel)}. \tag{37}$$

For each energy and transverse momentum vector, a separate set of equations for the Green's functions needs to be solved. For the charge carriers, the steady-state integro-differential equations derived from (13) and (14) read

$$G^R(\mathbf{k}_\parallel, z, z', E) = G_0^R(\mathbf{k}_\parallel, z, z', E) + \int dz_1 \int dz_2 \; G_0^R(\mathbf{k}_\parallel, z, z_1, E)\Sigma^R(\mathbf{k}_\parallel, z_1, z_2, E)G^R(\mathbf{k}_\parallel, z_2, z', E), \tag{38}$$

$$G^{\lessgtr}(\mathbf{k}_\parallel, z, z', E) = \int dz_1 \int dz_2 \; G^R(\mathbf{k}_\parallel, z, z_1, E)\Sigma^{\lessgtr}(\mathbf{k}_\parallel, z_1, z_2, E)G^A(\mathbf{k}_\parallel, z_2, z', E), \tag{39}$$

with

$$\left[E - \hat{\mathcal{H}}_0(\mathbf{k}_\parallel, z)\right] G_0^R(\mathbf{k}_\parallel, z, z', E) = \delta(z - z'). \tag{40}$$

The numerical evaluation of the above equations employs a real-space basis in the dimension perpendicular to the film, and a plane-wave expansion in the in-plane dimensions in combination with a two-band effective mass Hamiltonian for the electronic structure[25].

The Dyson and Keldysh equations for the dyadic photon Green's functions are found in analogy to their electronic counterparts in the following form (assuming again summation over repeated polarization indices):

$$\mathcal{D}_{\mu\nu}^R(\mathbf{q}_\parallel, z, z', E) = \mathcal{D}_{0\mu\nu}^R(\mathbf{q}_\parallel, z, z', E) + \int dz_1 \int dz_2 \mathcal{D}_{0\mu\alpha}^R(\mathbf{q}_\parallel, z, z_1, E)\Pi_{\alpha\beta}^R(\mathbf{q}_\parallel, z_1, z_2, E)\mathcal{D}_{\beta\nu}^R(\mathbf{q}_\parallel, z_2, z', E), \tag{41}$$

$$\mathcal{D}_{\mu\nu}^{\lessgtr}(\mathbf{q}_\parallel, z, z', E) = \int dz_1 \int dz_2 \mathcal{D}_{\mu\alpha}^R(\mathbf{q}_\parallel, z, z_1, E)\Big[\Pi_{0\alpha\beta}^{\lessgtr}(\mathbf{q}_\parallel, z_1, z_2, E) + \Pi_{\alpha\beta}^{\lessgtr}(\mathbf{q}_\parallel, z_1, z_2, E)\Big]\mathcal{D}_{\beta\nu}^A(\mathbf{q}_\parallel, z_2, z', E), \tag{42}$$

where the self-energy component related to the solution of the *homogeneous* problem, i.e., incident fluctuations that are independent from the state of the absorber, is given by[10,26]

$$\Pi_{0\mu\nu}^{\lessgtr}(\mathbf{q}_\parallel, z, z', E) = \int dz_1 \int dz_2 [\mathcal{D}_0^R]_{\mu\alpha}^{-1}(\mathbf{q}_\parallel, z, z_1, E) \times \mathcal{D}_{0\alpha\beta}^{\lessgtr}(\mathbf{q}_\parallel, z_1, z_2, E)[\mathcal{D}_0^A]_{\beta\nu}^{-1}(\mathbf{q}_\parallel, z_2, z', E) \tag{43}$$

in terms of the Green's functions of the unperturbed system. These equations are solved in real space using a numerical quadrature method[27].

The classical fields for the evaluation of the coherent self-energy (33) are computed using a conventional transfer matrix method (TMM), with extinction coefficient obtained from the absorption coefficient computed within the NEGF formalism, i.e., in complete consistency with the transport properties, such as the photocurrent generated via coupling to the EM field, as shown in the following.

B. Absorption and photogeneration

The local absorption coefficient at a fixed energy ($\sim E_\gamma$), polarization ($\sim \mu$) and angle of incidence ($\sim \mathbf{q}_\parallel,\ E_\gamma$) is related to the corresponding local and spectral photogeneration rate g (per unit volume) and local photon flux Φ (per unit photon energy) via

$$g^\mu(\mathbf{q}_\parallel, z, E_\gamma) = \Phi_\mu(\mathbf{q}_\parallel, z, E_\gamma)\alpha_\mu(\mathbf{q}_\parallel, z, E_\gamma). \tag{44}$$

The spectral photogeneration rate can be obtained from the expression for the local integral radiative interband volume generation rate $\mathcal{G}$ in terms of electronic Green's functions and self-energies[19], which for charge carriers in the CB reads

$$\mathcal{G}_c(z) = \mathcal{A}^{-1} \sum_{\mathbf{k}_\parallel} \int dz' \int \frac{dE}{2\pi\hbar} \Sigma_{cc}^{<}(\mathbf{k}_\parallel, z, z', E) \times G_{cc}^{>}(\mathbf{k}_\parallel, z', z, E) \tag{45}$$

$$\equiv \mathcal{A}^{-1} \sum_{\mu} \sum_{\mathbf{q}_\parallel} \int dE_\gamma \; g_c^\mu(\mathbf{q}_\parallel, z, E_\gamma). \tag{46}$$

In principle, the self-energy term contains all the scattering mechanisms present in the interaction part of the Hamiltonian (1). While the direct contribution of intraband scattering vanishes upon energy integration over the band, dissipative intraband processes, such as electron-phonon interaction, still affect the rate via the dressing of the full GF in (46). At the radiative limit, the photocurrent at zero bias voltage, i.e., the short circuit current density J_{sc}, is directly obtained from the incident photon flux and the total absorptance of the slab,

$$J_{sc} = \frac{e}{\mathcal{A}} \sum_{\mathbf{q}_\parallel} \int dE_\gamma \mathbf{\Phi}(\mathbf{q}_\parallel, z_0, E_\gamma) \cdot \mathbf{a}(\mathbf{q}_\parallel, z_{max}, E_\gamma), \tag{47}$$

where the absorptance corresponds to the external quantum efficiency $EQE(\mathbf{q}_\parallel, E_\gamma)$ in this limit. On the other hand, the short circuit current derives from the quantities

computed within the NEGF formalism as follows[19]:

$$J_{sc} = j_c(z_{max}) - j_c(z_0) = \int_{z_0}^{z_{max}} dz\ \partial_z j(z) \tag{48}$$

$$\equiv e \int_{z_0}^{z_{max}} dz\ \mathcal{G}_c(z), \tag{49}$$

where j_c denotes electron current in the conduction band, which is given terms of the charge carrier Green's functions via

$$j_c(z) = \lim_{z' \to z} \frac{e\hbar}{m_0}(\partial_z - \partial_{z'})\mathcal{A}^{-1} \sum_{\mathbf{k}_\parallel} \int \frac{dE}{2\pi} G^<_{cc}(\mathbf{k}_\parallel, z, z', E). \tag{50}$$

Together, Eqs. (47) and (49) yield the following expression of the absorptance in terms of the local generation spectrum:

$$a_\mu(\mathbf{q}_\parallel, z_{max}, E_\gamma) = \Phi_\mu^{-1}(\mathbf{q}_\parallel, z_0, E_\gamma) \int_{z_0}^{z_{max}} dz\ g^\mu(\mathbf{q}_\parallel, z, E_\gamma). \tag{51}$$

1. *Coupling to classical fields*

For classical fields, the local photon flux is given in terms of the modal components of the Poynting vector s and the electromagnetic vector potential in the following way:

$$\Phi_\mu(\mathbf{q}_\parallel, z, E_\gamma) = s^\mu(\mathbf{q}_\parallel, z, E_\gamma)/E_\gamma \tag{52}$$

$$= 2n_r(\mathbf{q}_\parallel, z, E_\gamma) c_0 \varepsilon_0 \hbar^{-2} E_\gamma |A_\mu(\mathbf{q}_\parallel, z, E_\gamma)|^2, \tag{53}$$

where n_r is the local refractive index. Using the electron-photon self-energy (33) in slab representation, i.e.,

$$\Sigma^<_{cc}(\mathbf{k}_\parallel, z, z', E) = \left(\frac{e}{m_0}\right)^2 \sum_{\mu\nu} p^\mu_{cv}(z) p^{\nu *}_{cv}(z') \times \mathcal{A}^{-1} \sum_{\mathbf{q}_\parallel} \int dE_\gamma \Big[A_\mu(\mathbf{q}_\parallel, z, E_\gamma) A^*_\nu(\mathbf{q}_\parallel, z', E_\gamma) \times \tilde{G}^<_{vv}(\mathbf{k}_\parallel - \mathbf{q}_\parallel, z, z', E - E_\gamma) \Big], \tag{54}$$

in expression (46) for $\mathcal{G}$, the local spectral photogeneration rate acquires the following form:

$$g^\mu(\mathbf{q}_\parallel, z, E_\gamma) = \frac{i}{\hbar\mu_0} A_\mu(\mathbf{q}_\parallel, z, E_\gamma) \int dz' A^*_\mu(\mathbf{q}_\parallel, z', E_\gamma) \times \Pi^>_{\mu\mu}(\mathbf{q}_\parallel, z', z, E_\gamma), \tag{55}$$

where Π is the photon self-energy related to the non-equilibrium polarization function of the semiconductor slab and the momentum matrix elements,

$$\Pi^>_{\mu\nu}(\mathbf{q}_\parallel, z, z', E_\gamma) = -i\hbar\mu_0 \left(\frac{e}{m_0}\right)^2 p^{\mu *}_{cv}(z) p^\nu_{cv}(z') \times \mathcal{P}^>_{cv}(\mathbf{q}_\parallel, z, z', E_\gamma), \tag{56}$$

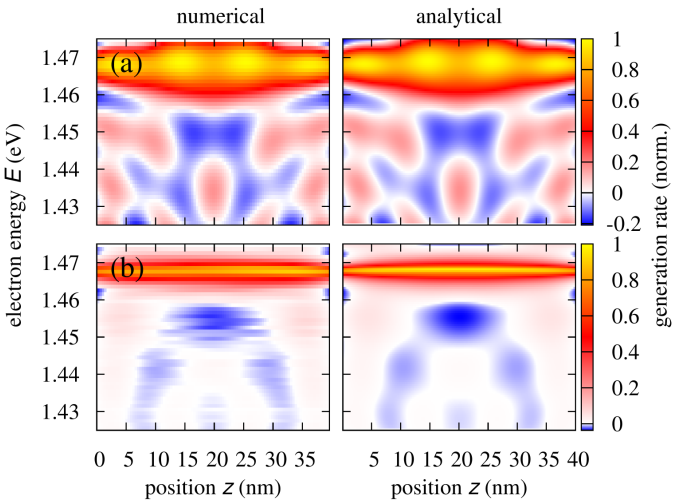

FIG. 2. (Color online) Local electron generation rate as given by the energy integrand of (46) for the two band effective mass model of a homogeneous (bulk-like) GaAs slab under monochromatic illumination with $E_\gamma = 1.48$ eV. The rate is normalized to the local photon flux and to the maximum value. Both the $k_\parallel = 0$ component (a) and the momentum integrated rate (b) show a good agreement between the simulation based on the numerical solution of the NEGF transport problem at zero bias and the analytical evaluation of (46) using the exact GF expressions (A1) and (A2).

with the RPA interband polarization function given in terms of the charge carrier GF as follows:

$$\mathcal{P}^>_{cv}(\mathbf{q}_\parallel, z, z', E_\gamma) = \mathcal{A}^{-1} \sum_{\mathbf{k}_\parallel} \int \frac{dE}{2\pi\hbar} G^>_{cc}(\mathbf{k}_\parallel, z, z', E) \times G^<_{vv}(\mathbf{k}_\parallel - \mathbf{q}_\parallel, z', z, E - E_\gamma). \tag{57}$$

The absorptance of the slab of thickness $d = z_{max} - z_0$ required for the optical estimate of the short circuit current via (47) is thus given by

$$a_\mu(\mathbf{q}_\parallel, z_{max}, E_\gamma) = \Phi_\mu^{-1}(\mathbf{q}_\parallel, z_0, E_\gamma) \times \frac{i}{\hbar\mu_0} \int_{z_0}^{z_{max}} dz \int_{z_0}^{z_{max}} dz' \Big[A_\mu(\mathbf{q}_\parallel, z, E_\gamma) \times A^*_\mu(\mathbf{q}_\parallel, z', E_\gamma) \Pi^>_{\mu\mu}(\mathbf{q}_\parallel, z', z, E_\gamma) \Big]. \tag{58}$$

To verify the accuracy of the numerical approach chosen to compute the microscopic non-local response of a thin semiconductor slab, the numerical generation rate is compared to the analytical result for the integrand of (57) based on the exact Green's functions of homogeneous bulk material given in the Appendix. The material parameters used are $m_c = 0.067\ m_0$, $m_v = 0.25\ m_0$, $E_g = 1.42$ eV $\equiv E_{c0}$, $E_{v0} = 0$ eV and $|\bar{p}_{cv}|^2 = 25$ eV$\cdot\ m_0$. Fig. 2(a) shows the $k_\parallel = 0$ component of the local electron generation rate spectrum for monochromatic illuminaton normalized to the local photon flux, which then

basically amounts to the evaluation of the energy integrand of the polarization function (57) at photon energy $E_\gamma = 1.48$ eV. The spectral and spatial pattern are in excellent agreement with the analytical high-resolution result. The same holds for the $\mathbf{k}_\parallel$-integration of the spectral rate, as inferred from Fig. 2(b).

In most cases relevant for optoelectronic devices, the electronic spatial correlations, i.e., the off-diagonal elements of the interband polarization function, decay much faster than the amplitude of the vector potential inside the absorber, and $A(z') \approx A(z)$ can be assumed in (55). In this case, the local absorption coefficient acquires the simple form

$$\alpha_\mu(\mathbf{q}_\parallel, z, E_\gamma) = \frac{\hbar c_0}{2n_r(\mathbf{q}_\parallel, z, E_\gamma)E_\gamma} \times \int dz' \mathrm{Re}\Big[i\Pi^{>}_{\mu\mu}(\mathbf{q}_\parallel, z', z, E_\gamma)\Big] \quad (59)$$

$$= \frac{\hbar^2}{2n_r(\mathbf{q}_\parallel, z, E_\gamma)c_0\varepsilon_0 E_\gamma}\Big(\frac{e}{m_0}\Big)^2 \mathrm{Re}\Big[p^\mu_{cv}(z) \times \int dz' p^{\mu *}_{cv}(z')\mathcal{P}^{>}_{cv}(\mathbf{q}_\parallel, z', z, E_\gamma)\Big], \quad (60)$$

which is given solely in terms of the electronic structure and does not include any information on the propagation of the light. However, the inclusion of off-diagonal elements in the electronic Green's functions is crucial to account for the non-local nature of electron-photon interaction[28]. Figure 3(a) shows the spatially averaged local absorption coefficient of a homogeneous GaAs slab of 40 nm thickness for different numbers of off-diagonals considered in the electronic Green's functions: more than 20% of the off-diagonals need to be included for an acceptable reproduction of the full rank result. For the slab thickness chosen, the full matrix yields already an absorption coefficient in close agreement with the analytical bulk result for the two-band model, as seen in Fig. 3(b). The spatial resolution of the local absorption coefficient is given in Fig. 3(c) for the bulk-like system ("open") and the slab with carrier selective contacts ("selective"). The minimum of the absorption of the open system close to the contacts is due to the assumption of vanishing off-diagonal contributions to the polarization function in (57) from outside the slab, i.e., it assumed that there is no coherence between the carrier wave functions inside the slab absorber and in the contact, respectively. In the system with selective contacts, either electron or hole Green's functions vanish at the contacts, causing nodes in the local absorption coefficient.

The absorptance can also be computed directly from the Poynting vector based on the fields obtained from the TMM,

$$a_\mu(\mathbf{q}_\parallel, z_{max}, E_\gamma) = 1 - s^\mu(\mathbf{q}_\parallel, z_{max}, E_\gamma)/s^\mu(\mathbf{q}_\parallel, z_0, E_\gamma), \quad (61)$$

for flux incident at $z = z_0$. Figure 3(c) shows the close agreement between the monochromatic photocurrent from the absorptance as given by the integrand of

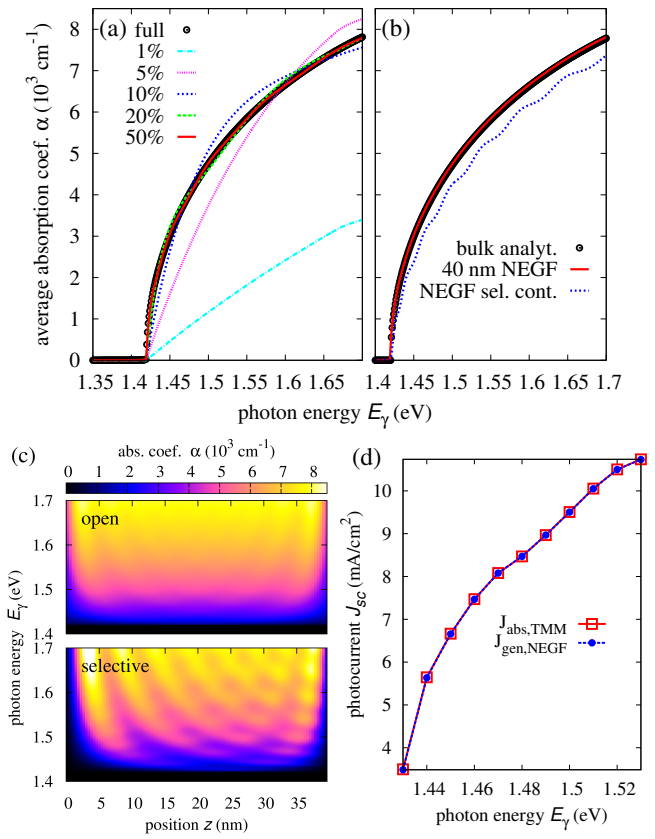

FIG. 3. (Color online) (a) Spatially averaged absorption coefficient of an electronically open 40-nm-thick GaAs slab, for consideration of different fractions of off-diagonals in the charge carrier Green's functions. (b) The absorption coefficient from the full matrix is in excellent agreement with the analytical result for bulk, while it is slightly reduced and shows additional oscillatory features for selective contacts. (c) Local absorption coefficient for open and selectively contacted slab systems, with interferences from reflections and zero magnitude minima from wave function nodes at closed contacts. (d) Comparison of the photocurrent as obtained from the absorptance with the terminal current from the full NEGF transport simulation based on the same illumination and extinction coefficient.

(47) and the terminal current obtained from the NEGF for the same monochromatic illumination, using in the TMM an extinction coefficient computed from the electronic structure in consistence with a via

$$\kappa_\mu(\mathbf{q}_\parallel, z, E_\gamma) = \alpha_\mu(\mathbf{q}_\parallel, z, E_\gamma) \cdot \frac{\hbar c_0}{2E_\gamma} \quad (62)$$

$$= \frac{(\hbar c_0)^2}{4n_r(\mathbf{q}_\parallel, z, E_\gamma)E_\gamma^2} \times \int dz' \mathrm{Re}\Big[i\Pi^{>}_{\mu\mu}(\mathbf{q}_\parallel, z', z, E_\gamma)\Big] \quad (63)$$

and for a 100 nm Ag back reflector ($n_r = 0.16$, $\kappa = 5.85$).

The proper generation rate under consideration of the spatial variation of the electromagnetic field inside the

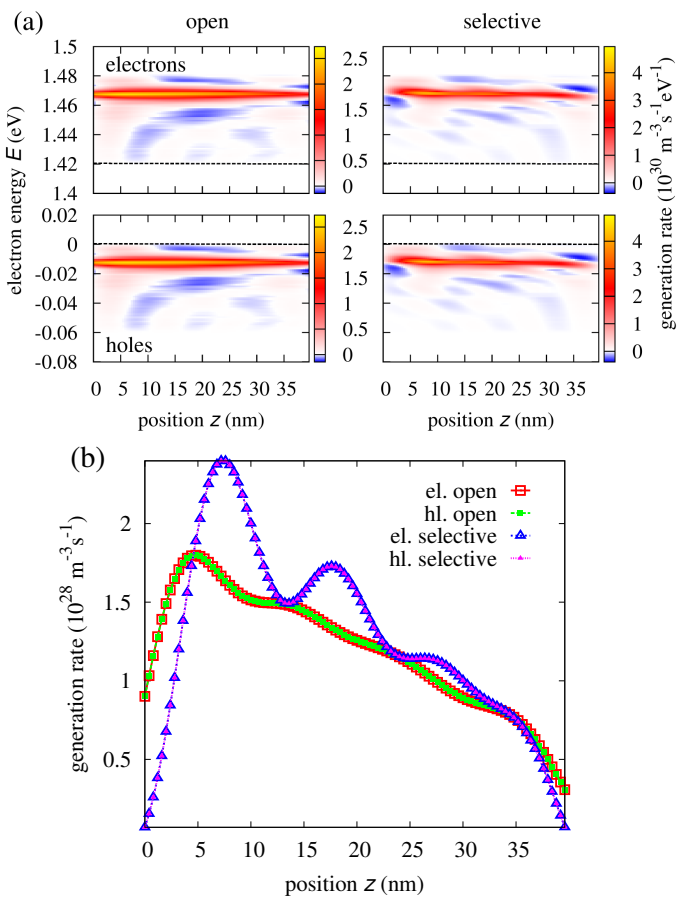

FIG. 4. (Color online) (a) Local generation rate spectrum for open and selectively contacted 40 nm GaAs slab with 100 nm Ag reflector and under monochromatic, normally incident light of 1 kW/m^2 at $E_\gamma = 1.48$ eV; (b) Integrated local carrier generation rate, which is identical for electrons and holes, with closed contacts resulting in reflection-induced interference effects and boundary nodes.

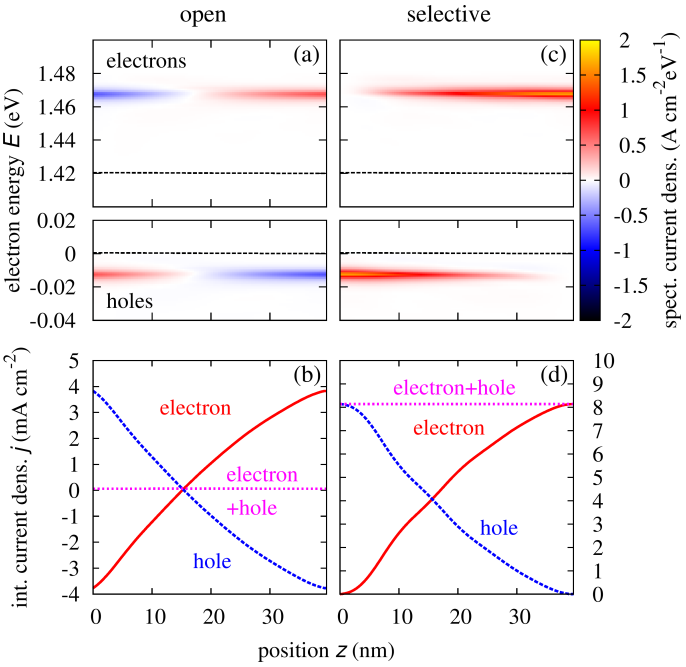

FIG. 5. (Color online) (a) Spatially resolved photocurrent spectrum for the open slab under monochromatic illumination of 1 kW/m^2 with $E_\gamma = 1.48$ eV; in the absence of carrier selective contacts, diffusion leads to inverse current flow towards the minority contacts, with the result of vanishing net current upon energy integration as displayed in (b). (c) For carrier selective contacts, reverse current components are small, and the net integral current (d) is strictly positive and perfectly conserved.

slab is shown in Fig. 4 for both the bulk-like slab and the system with carrier-selective contacts under monochromatic illumination at $E_\gamma = 1.48$ eV, 1 kW/m^2 and normal incidence. The spectral generation patterns shown in Fig. 4(a) are identical for electrons and holes, and show weak negative features away from the resonance. However, the energy-integrated local generation rate, displayed in Fig. 4(b) is strictly positive. Again, the imposition of carrier-selective contacts modifies the local absorption due to additional interferences from reflections and magnitude zeros from wave function nodes at closed contacts.

The local photocurrent spectrum induced in the open bulk-like slab system by the local carrier generation rate is displayed in Fig. 5(a). In the absence of carrier selective contacts, carriers diffuse symmetrically in both directions, with the result of vanishing net integral current [Fig. 5(b)]. For the selectively contacted system, the negative contributions in the generation rate give rise to reverse flow at certain energies (this was also observed for purely 1D systems in Ref. 29), as revealed in Fig. 5(c), however, like in the case of the generation rate, the observable integral current is always positive and the sum of electron and hole current contributions is perfectly conserved, as shown in Fig. 5(d).

2. *Coupling to the photon GF*

Using the slab-expression for the steady-state RPA electron-photon self-energy,

$$\Sigma^{\lessgtr}(\mathbf{k}_\parallel, z, z', E) = i\hbar\mu_0 \left(\frac{e}{m_0}\right)^2 \sum_{\mu\nu} \hat{p}^\mu(z)\hat{p}^{\nu *}(z') \times \mathcal{A}^{-1} \sum_{\mathbf{q}_\parallel} \int \frac{dE_\gamma}{2\pi\hbar} \Big[G^{\lessgtr}(\mathbf{k}_\parallel - \mathbf{q}_\parallel, z, z', E - E_\gamma) \times \mathcal{D}^{\lessgtr}_{\mu\nu}(\mathbf{q}_\parallel, z, z', E_\gamma) \Big], \quad (64)$$

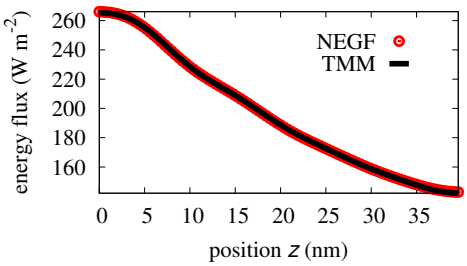

FIG. 6. (Color online) Photon energy flux in the selectively contacted slab as computed via TMM and NEGF methods, showing the close agreement of the two approaches for coherent light propagation, i.e., in absence of spontaneous emission.

in Eq. (46), the local modal generation rate acquires the following form:

$$g^{\mu}(\mathbf{q}_{\parallel},z,E_{\gamma}) = -(2\pi\hbar)^{-1}\sum_{\nu}\int dz'\Big[\mathcal{D}^{<}_{\mu\nu}(\mathbf{q}_{\parallel},z,z',E_{\gamma}) \times \Pi^{>}_{\nu\mu}(\mathbf{q}_{\parallel},z',z,E_{\gamma})\Big]. \quad (65)$$

In terms of the photon slab Green's functions defined in (37), the contribution of the μ-polarization to the z-component of the spectral Poynting vector reads

$$s^{\mu}_{z}(\mathbf{q}_{\parallel},z,E_{\gamma}) = -\frac{E_{\gamma}}{2\pi\hbar}\lim_{z'\to z}\partial_{z'}\mathrm{Re}\Big[\mathcal{D}^{>}_{\mu\mu}(\mathbf{q}_{\parallel},z,z',E_{\gamma}) + \mathcal{D}^{<}_{\mu\mu}(\mathbf{q}_{\parallel},z,z',E_{\gamma})\Big]. \quad (66)$$

Figure 6 shows the close agreement of the optical energy flux as computed via TMM and the photon NEGF formalism with fully non-local photon self-energy Π[27]. From the modal terms of local rate and photon flux, the local absorption coefficient at given angle of incidence and polarization is then given by (44) with $\Phi_{\mu}(\mathbf{q}_{\parallel},z,E_{\gamma}) = s^{\mu}_{z}(\mathbf{q}_{\parallel},z,E_{\gamma})/E_{\gamma}$, and from (51), the absorptance follows as

$$a_{\mu}(\mathbf{q}_{\parallel},z_{max},E_{\gamma}) = -\big[2\pi\hbar\,\Phi_{\mu}(\mathbf{q}_{\parallel},z_0,E_{\gamma})\big]^{-1} \times\int_{z_0}^{z_{max}}dz\int_{z_0}^{z_{max}}dz'\sum_{\nu}\Big[\mathcal{D}^{<}_{\mu\nu}(\mathbf{q}_{\parallel},z,z',E_{\gamma}) \times\Pi^{>}_{\nu\mu}(\mathbf{q}_{\parallel},z',z,E_{\gamma})\Big]. \quad (67)$$

It should be noted that the above expression for the absorptance does not consider any increase in the photon flux due to emission processes; to that end, the self-energy component $\Pi^{>}$ needs to be replaced by $\hat{\Pi} = \Pi^{>} - \Pi^{<}$[10], which for the present case of short circuit conditions is virtually identical to $\Pi^{>}$. If reabsorption is neglected, the GF component $\mathcal{D}^{<}$ is directly proportional to the photon flux via $\mathcal{D}^{<}_{0} = \hat{\mathcal{D}}_0\cdot\Phi_0$, where $\hat{\mathcal{D}}_0$ is independent from the excitation due to the photon flux Φ_0 incident at $z = z_0$[27]. With that, the absorptance

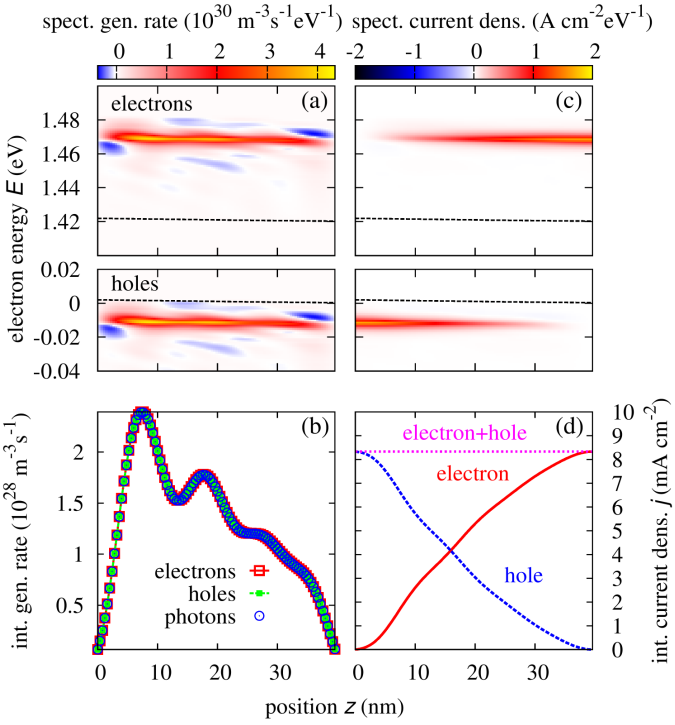

FIG. 7. (color online) (a) Local charge carrier generation rate spectrum, (b) local carrier generation rate and optical rate, (c) local charge carrier current spectrum and (d) integral current for the selectively contacted slab system, as provided by the NEGF formalism using the coupling to the photon GF. The results are in close agreement with those from the coherent coupling approximation. The local charge carrier generation rate concides exactly with the optical rate from photon self-energy and GF.

acquires the form

$$a_{\mu}(\mathbf{q}_{\parallel},z_{max},E_{\gamma}) = -(2\pi\hbar)^{-1} \times\int_{z_0}^{z_{max}}dz\int_{z_0}^{z_{max}}dz'\sum_{\nu}\Big[\hat{\mathcal{D}}_{\mu\nu}(\mathbf{q}_{\parallel},z,z',E_{\gamma}) \times\hat{\Pi}_{\nu\mu}(\mathbf{q}_{\parallel},z',z,E_{\gamma})\Big], \quad (68)$$

where $\hat{\boldsymbol{\mathcal{D}}} = \boldsymbol{\mathcal{D}}^{R}\boldsymbol{\mathcal{D}}_0^{R,-1}\hat{\boldsymbol{\mathcal{D}}}_0\boldsymbol{\mathcal{D}}_0^{A,-1}\boldsymbol{\mathcal{D}}^{A}$. This corresponds to the result found in Ref. 10.

The numerical results for local generation rate and charge carrier flow in the selectively contacted slab for coupling to the photon GF are displayed in Fig. 7. As can be inferred from Figs. 7(a) and 7(b) in comparison with Fig. 4, the values of spectral and integral charge carrier generation rates agree closely with those provided by the coherent coupling. The same holds for the spectral and integral currents displayed in Figs. 7(c) and 7(d), if compared to the results in Fig. 5. Furthermore, as also shown in Fig. 7(b), the charge carrier generation rate coincides exactly with the optical rate as computed using (65), i.e., in terms of the photon GF and self-energy.

The coincidence with the coherent coupling approximation originates in the absence of (optical) coherence breaking mechanisms in the situation under consideration, direct photogeneration being a stimulated process. The photon GF can thus be directly related to the average fields[10,16]. This may be compared to the case of electron transport in mesoscopic systems, where in absence of phase breaking, i.e., incoherent scattering mechanisms, the Landauer formalism based on a transmission function obtained from an electronic version of the TMM is equivalent to the NEGF picture of electron transport[6].

V. CONCLUSIONS

In this paper, a description of charge carrier photogeneration in thin semiconductor films within the NEGF formalism was established. An effective electron-photon self-energy was derived for coherent coupling to classical fields. Numerical simulations were performed for a thin, selectively contacted semiconductor slab with a back reflector. The results for charge carrier generation rate and photocurrent computed using the NEGF formalism of carrier transport coupled to the TMM for the electromagnetic fields are in close agreement with the predictions of both the optical estimate via the average absorption coefficient and the full coupled NEGF solution for the propagation of interacting charge carriers and photons. Thus, the NEGF framework presented here is consistent with the classical picture of light-matter coupling in the limit of optically coherent processes, and, at the same time, enables the consideration of both extraction and radiative recombination of charge carriers in the presence of complex nanostructure potentials. This unique capability turns the present approach into a powerful instrument for the investigation of the radiative efficiency limit in nanostructure-based solar cell devices.

For a quantitative analysis of photocurrent generation in realistic device structures, in addition to the use of an accurate description of the electronic structure, extension of the formalism to radiative intraband mechanisms (e.g., free carrier absorption) and non-radiative intra- and interband scattering processes (e.g., electron-phonon and Auger) will be required. The inclusion of such processes, however, while it modifies the GF and self-energies of charge carriers and photons, it does not affect the validity of the general expressions derived here for absorptance, generation rate and photocurrent in terms of the GF.

ACKNOWLEDGMENTS

The author would like to acknowledge the support and kind hospitality of the National Renewable Energy Laboratory in Golden, Colorado, USA, during his visit in the framework of the Helmholtz-NREL Joint Research Initiative HNSEI.

Appendix A: Electronic Green's functions for homogeneous slab

For a homogeneous bulk-like system, the effective mass approximation of the slab representation of the steady-state Green's function components for non-interacting charge carriers in quasi-equilibrium conditions characterized by a quasi-Fermi level μ takes the following form:

$$G^{<}_{b0}(\mathbf{k}_\parallel, z, z', E) = i f_{\mu_b}(E) A_{b0}(\mathbf{k}_\parallel, z, z', E), \tag{A1}$$

$$G^{>}_{b0}(\mathbf{k}_\parallel, z, z', E) = -i[1 - f_{\mu}(E)] A_{b0}(\mathbf{k}_\parallel, z, z', E), \tag{A2}$$

$$A_{b0}(\mathbf{k}_\parallel, z, z', E) = \frac{2m^*_b}{\hbar^2} \frac{\cos[k^b_z(\mathbf{k}_\parallel, E)(z - z')]}{k^b_z(\mathbf{k}_\parallel, E)}, \tag{A3}$$

where

$$k^b_z(\mathbf{k}_\parallel, E) = \sqrt{2m^*_b E - \hbar^2 k^2_\parallel}/\hbar, \quad b = c, v, \tag{A4}$$

$$f_\mu(E) = \left\{ \exp[(E - \mu)/k_B T] + 1 \right\}^{-1}. \tag{A5}$$

* u.aeberhard@fz-juelich.de

1. H. Haug and S. W. Koch, *Quantum Theory of the Optical and Electronic Properties of Semiconductors* (World Scientific, 2004).
2. U. Aeberhard, J. Comput. Electron. **10**, 394 (2011).
3. U. Aeberhard, IEEE J. Sel. Topics in Quantum Electron. **19**, 4000411 (2013).
4. W. Schäfer and M. Wegener, *Semiconductor Optics and Transport Phenomena* (Springer, Berlin, 2002).
5. M. Kira and S. W. Koch, Phys. Rev. A **73**, 013813 (2006).
6. S. Datta, *Electronic Transport in Mesoscopic Systems* (Cambridge University Press, 1995).
7. S. Datta, *Quantum Transport* (Cambridge University Press, 2005).
8. U. Aeberhard and R. H. Morf, Phys. Rev. B **77**, 125343 (2008).
9. L. Keldysh, Sov. Phys. JETP **20**, 1018 (1965).
10. F. Richter, M. Florian, and K. Henneberger, Phys. Rev. B **78**, 205114 (2008).
11. M. F. Pereira and K. Henneberger, Phys. Rev. B **53**, 16485 (1996).
12. M. F. Pereira and K. Henneberger, Phys. Rev. B **58**, 2064 (1998).
13. D. F. DuBois, *Nonequilibrium quantum statistical mechanics of plasmas and radiation*, edited by W. Brittin, Lectures in theoretical physics, Vol. 109 (Gordon and Breach, New York, 1967) Chap. Nonequilibrium quantum statistical mechanics of plasmas and radiation, pp. 469–620.
14. K. Henneberger and H. Haug, Phys. Rev. B **38**, 9759 (1988).
15. F. Jahnke and S. W. Koch, Phys. Rev. A **52**, 1712 (1995).

[16] K. Henneberger and S. W. Koch, Phys. Rev. Lett. **76**, 1820 (1996).
[17] Intraband transitions such as free carrier absorption are explicitely excluded at this stage.
[18] K. Henneberger, Physica A **150**, 419 (1988).
[19] U. Aeberhard, Phys. Rev. B **84**, 035454 (2011).
[20] If the singular part of the electron-electron interaction is included, the singular self-energy is no longer local in space and spatial integration should also be performed.
[21] L. P. Kadanoff and G. Baym, *Quantum Statistical Mechanics* (Benjamin, Reading, Mass., 1962).
[22] D. Langreth, in *Linear and Non-linear Electron Transport in solids* **17**, 3 (1976).
[23] P. Würfel, *Physics of Solar Cells* (Wiley-VCH, 2005).
[24] U. Aeberhard, Opt. Quantum. Electron. **44**, 133 (2012).
[25] U. Aeberhard, Nanoscale Res. Lett. **6**, 242 (2011).
[26] D. Mozyrsky and I. Martin, Opt. Commun. **277**, 109 (2007).
[27] U. Aeberhard, "Simulation of light propagation in thin semiconductor films with non-local electron-photon interaction," Unpublished, arXiv:1308.3159 [cond-mat.mes-hall].
[28] M. Pourfath and H. Kosina, Journal of Computational Electronics **8**, 427 (2009).
[29] A. Buin, A. Verma, and S. Saini, J. Appl. Phys. **114**, 033111 (2013).